Effect of carbonization temperature on the physical and electrochemical properties of supercapacitor electrode from fibers of oil palm empty fruit bunches

M. M. Ishak, M. Deraman, I. A. Talib, N. H. Basri, Awitdrus, R. Farma, E. Taer, R. Omar, N. S. M. Nor, and B. N. M. Dolah

Articles you may be interested in

Effect of electrolyte concentration on performance of supercapacitor carbon electrode from fibers of oil palm empty fruit bunches
AIP Conf. Proc. **1656**, 030006 (2015); 10.1063/1.4917095

Nanoporous separators for supercapacitor using activated carbon monolith electrode from oil palm empty fruit bunches
AIP Conf. Proc. **1586**, 68 (2014); 10.1063/1.4866732

Production of succinic acid from oil palm empty fruit bunch cellulose using Actinobacillus succinogenes
AIP Conf. Proc. **1571**, 753 (2013); 10.1063/1.4858745

Carbon/Carbon Nanotubes (CNTs) Composites from Green Pellets Contain CNTs and Self-adhesive Carbon Grains from Fibres of Oil Palm Empty Fruit Bunch
AIP Conf. Proc. **1284**, 179 (2010); 10.1063/1.3515546

Effect of Reinforcement Shape and Fiber Treatment on the Mechanical Properties of Oil Palm Empty Fruit Bunch-Polyethylene Composites
AIP Conf. Proc. **1217**, 335 (2010); 10.1063/1.3377839

Effect of Carbonization Temperature on The Physical and Electrochemical Properties of Supercapacitor Electrode from Fibers of Oil Palm Empty Fruit Bunches

M. M. Ishak[1], M. Deraman,[1*], I. A. Talib[1], N. H. Basri[1], Awitdrus[1,2], R. Farma[1,2], E. Taer[1,2], R. Omar[1], N. S. M. Nor[1] and B. N. M. Dolah[1]

[1]*School of Applied Physics, Faculty of Science and Technology, Universiti Kebangsaan Malaysia, 43600 Bangi, Selangor, Malaysia*
[2]*Department of Physics, Faculty of Mathematics and Natural Sciences, University of Riau, 28293 Pekanbaru, Riau, Indonesia*
*Email: madra@ukm.my

Abstract. Self-adhesive carbon grains (SACG) was prepared from fibers of oil palm empty fruit bunches. The SACG green monoliths were carbonized in N_2 environment at 400, 500, 600 and 700°C to produce carbon monoliths labeled as CM1, CM2, CM3 and CM4 respectively. The CMs were activated in CO_2 surrounding at 800°C for 1 hour to produce activated carbon monolith electrodes (ACM1, ACM2, ACM3 and ACM4). The physical properties of the CMs and ACMs were investigated using X-ray diffraction, field emission scanning electron microscopy (FESEM) and N_2 adsorption-desorption isotherm techniques. ACMs were used as electrode to fabricate symmetry supercapacitor cells and the cells' performances were investigated using electrochemical impedance spectroscopy (EIS), cyclic voltammetry (CV) and galvanostatic charge-discharge (GCD) standard techniques. In this paper we report the physical and electrochemical properties of the ACM electrodes by analyzing the influence of the carbonization temperature on these properties.

Keywords: Activated carbon monoliths, Supercapacitor, Electrochemical properties, Porosity, Microstructure.
PACS: 81.05.U-, 82.47.Uv, 92.60.hv, 68.43.-h, 84.37.+q

INTRODUCTION

Supercapacitor is a device which can store energy based on the electrostatic charge storage mechanism involving electrical double layer formed at the interface between electrode and electrolyte [1]. This double layer is formed by ionic charges from electrolyte and electronic charges from electrode. A very small distance (a few nm depending on the diameter of the ion of electrolyte solution used) between ionic and electronic charges, and a large electrode surface area are the important factors that make supercapacitor having larger energy storage capability compared to conventional capacitor [2]. However, its energy storage capability is still inferior compared to that of the batteries. Supercapacitor is being widely used in electric/hybrid vehicles, telecommunication devices, digital communication systems, digital cameras and laser pulse technique [3,4].

A large electrode surface area can be achieved by having a large quantities of micropores in electrode material and this is very important because large surface area will allow a larger amount of charges to accumulate and hence give rise to higher capacitance or energy values [1,4]. An appropriate selection of the supercapacitor carbon electrode with desired characteristics can be obtained from an activated carbon produced from a variety of low cost biomass [5]. Activated carbon is a porous material whose pore size in the nanometer scale can be controlled by both physical and chemical treatments during its production. The physical treatment involves two major steps processes (i) the carbonization process (CP), and followed by (ii) activation process (AP) under certain conditions such as sample environment condition (for example in CO_2 environment), activation temperature and activation time [2].

In the present study, the green monoliths (GM) of self-adhesive carbon grain (SACG) were prepared from fibers of oil palm empty fruit bunches (EFB) and converted into carbon monolith by carbonization process up to four different carbonization temperatures (400, 500, 600, 700°C) prior to activation with CO_2 to produce activated carbon electrodes for supercapacitor application. Structural, microstructure, porosity and electrochemical properties of electrodes were studied in terms of their dependence on the carbonization temperature.

EXPERIMENTAL

EFB (Ecofibre Technology Sdn. Bhd.) was converted into SACG with particle size ≤ 53 μm by low temperature pre-carbonization (280°C), grinding, milling and sieving based on the method reported earlier [6]. SACG was then pelletized into monolith shape and carbonized at four different temperatures 400, 500, 600 and 700°C in N_2 environment (1.5 l/min). Carbonized monoliths were activated in CO_2 (1.0 l/min) environment at 800°C for 1 h to produce activated carbon monoliths (ACMs) with a dimension of 14.92 to 15.27 mm diameter, 1.5467 to 1.63 mm thickness and 0.26617 to 2.9970 g mass. The ACMs were polished to produce electrodes with thickness of ~0.4 mm.

The X-ray diffraction measurement over an angular range of 2θ from 10° to 70° with a step size of 0.025^o were conducted on ACMs using a diffractometer (Bruker AXS : model D8 Advance, which employed Cu anode with the $K_{\alpha 1}$ of 1.5406 Å wavelength). The microcrystallites parameters, i.e. stack height (L_c) and width (L_a) of microcrystallites of the ACMs were determined from the diffraction peaks (002) and (100) using equations stated in [7] and the interlayer spacing (d) of the ACMs were calculated using the Bragg's Law from the (002) and (100) diffraction peaks. Microstructure of the ACMs was investigated using field emission scanning electron microscopy (FESEM) (Supra PV 55 model). Porosity parameters (BET surface area (S_{BET}), surface area of micropore (S_{Micro}), surface area of micropore (S_{Meso}), mesopore volume (V_{Meso}), micropore volume (V_{Micro}) and average pore diameter (D)) were obtained from N_2 adsorption-desorption isotherm measurements at 77 K using accelerated surface area and porosimeter system (ASAP 2010 Micromeretics).

Symmetrical supercapacitor cells were fabricated using ACMs electrodes, a pair of current collectors (stainless steel 316L), sulfuric acid (1M) as an electrolyte and teflon of thickness 0.2 mm as a separator. Characterization of the performance of supercapacitor cell was carried out using electrochemical impedance spectroscopy (EIS), cyclic voltammetry (CV) and galvanic charge-discharge (GCD) methods. The instrument used was a Solartron 1286 electrochemical interface and Solartron 1255HF frequency response analyzer. The specific capacitance of the electrode can be calculated using expression (1) to (3) from the EIS, CV and GCD data, respectively [9]

$$C_{sp} = -\frac{1}{\pi f Z'' m} \quad (1)$$

$$C_{sp} = \frac{2i}{Sm} \quad (2)$$

$$C_{sp} = \frac{2i'}{\left(\frac{\Delta V}{\Delta t}\right)m} \quad (3)$$

where f is the frequency, Z" is the imaginary impedance, i is the electric current, S is the scan rate, ΔV is the voltage different, Δt is the discharge period, i' is the current density and m is the mass. The specific energy and specific power were calculated from GCD data and calculated using equations (4) and (5), respectively

$$E = \frac{Vit}{m} \quad (4)$$

$$P = \frac{Vi}{m} \quad (5)$$

where V is the voltage, i is the current and t is the time.

RESULTS AND DISCUSSIONS

X-ray diffractogram (Figure 1) of each ACM has two broad peaks at 2θ of about 23°-24° and 43°-44° respectively, corresponding to the diffraction peaks (002) and (100) which indicates that all ACM have turbostratic structure [7,8]. The values of microcrystallite parameters, L_c, L_a, the ratio L_c/L_a, and d correspond to the diffraction peaks (002) and (100) respectively, calculated from the X-ray data, are listed in Table 1. The ratio of L_c/L_a has been reported to be proportional to the value of specific capacitance [10].
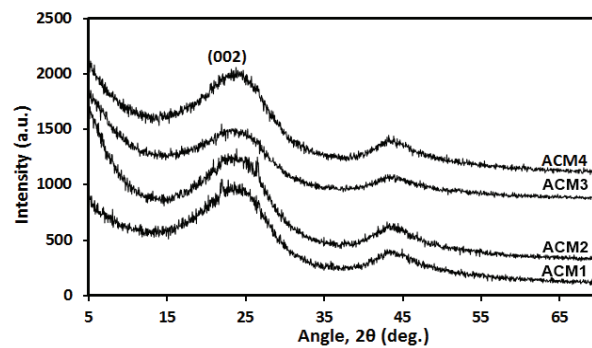

FIGURE 1. X-ray diffractogram for all ACMs.

FESEM micrographs with the magnification of 100kX for the fractured surface of ACMs sample with the electrodes have a very porous microstructure but the fractured surface of ACM1 and ACM2 seem to be more rough than the other two samples, indicating the effect of changing the carbonization temperature on the microstructure of the electrodes.

TABLE 1. Interlayer spacing and microcrystallite parameters values for all ACMs

Carbonization temperatures (^{o}C)	X-Ray data				Microcrystallite parameters		L_c/L_a
	$2\theta_{002}$(deg.)	$2\theta_{100}$(deg.)	d_{002}(Å)	d_{100}(Å)	L_c(Å)	L_a(Å)	
400	23.687	43.887	3.7536	2.062	10.84	46.21	0.235
500	23.821	44.814	3.7328	2.021	10.91	22.79	0.379
600	23.697	44.766	3.7520	2.023	11.40	32.90	0.347
700	23.732	44.384	3.7455	2.040	10.44	34.77	0.300

Figure 3 shows the results of N_2 adsorption-desorption isotherm measurements at 77 K for all of the ACMs electrodes. All of the electrodes show a common adsorption-desorption profile of type IV (based on IUPAC characterization [11]) with a hysteresis loop at $P/P_o > 0.4$ which has characteristic of samples with micropores and mesopores [12], with a clear different in the level of their adsorption-desorption capacity. This indicates a significant effect of carbonization temperature on the development of electrode porosity during activation. The data were analysed further by calculating the BET surface area (S_{BET}) and the micro pore surface area (S_{micro}) using the Brunauer-Emmett-Teller (BET) equation and t-plot method. The results obtained are shown in Table 2 and it can be expected that the pore characteristic vary with the carbonization temperature. A similar study was reported on carbon from corncob, where carbonization temperature selected from 300 to 800^oC for activation at 800^oC produced S_{BET} value from 728 - 986 m^2/g [13].

Comparison of Nyquist plots in Figure 4 among all the cells show that the carbonization temperature has affected the electrochemical properties of the electrodes since plot profile details differ from one another. This plot can be interpreted based on three ranges of frequency (i) high frequency (100k<f<79.43 Hz) -a semicircle that represents a domination of resistance in the cell, (ii) medium-high frequency (1k<f <0.0631 Hz) -a straight line with approximately 45° angle to the horizontal plane or the Warburg resistance caused by the entry of ions into the micro pores and increase capacitance by increasing the entry of ions into the pores, and (iii) low frequency (0.25119<f <0.01 Hz) -an almost vertical straight line represents the capacitance resulted from the double layer system of ionic charge from the electrolyte and the electronic charge from the electrodes on the surface of the micropores due to the effectiveness of the entry of ions into the pores in this range of frequencies. Semicircle portion begins with the first x-axis intercept, R_s, which is the resistance caused by the electrolyte and interface between electrode and current collector, while the second x-axis intercept, R_p is the intrinsic resistance of the electrode [10,14]. As can be seen in Table 3, R_p is more dependent on the carbonization temperature, which is an expected

behavior because the intrinsic resistance of electrodes is highly related to the pore characteristic of the electrodes. Similarly for the Z" value, it shows a significant variation with the carbonization temperature, with the lowest value exhibited by the ACM2 electrode, that is corresponding the highest specific capacitance value (calculated using equation (1)).
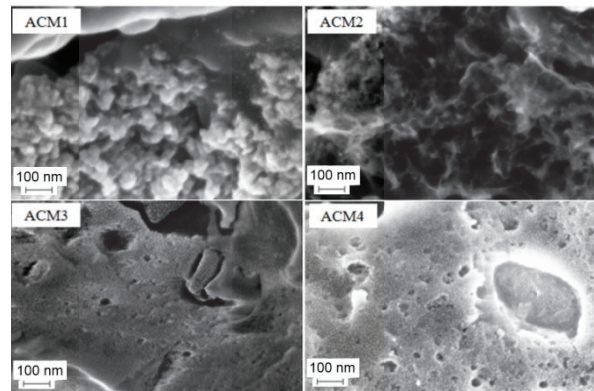
FIGURE 2. FESEM micrographs for all ACMs.
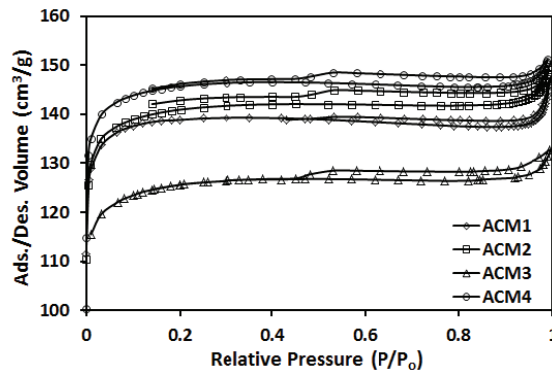
FIGURE 3. N_2 adsorption-desorption isotherm for all ACMs.

Figures 5 (a) and (b) respectively compare the dependence of real and imaginary parts of capacitance on the frequency among all the cells. The ACM2 cells seems to be superior than other cells throughout all the frequency range and is highly dependent on frequency, indicating the existence of an optimum carbonization temperature (~500 ^{o}C). For the imaginary part, each curve consists of peak associated with the peak frequency, f_p, which is the maximum frequency can be

sustained by the dominance capacitive behavior [14]. The relaxation time (τ_o) can give an estimation of power capacity because the power inversely proportional to the (τ_o) [16]. The values of (τ_o) in Table 3 are in agreement with the power capacity shown in Ragone plot (Figure 8).

TABLE 2. Porosity parameters values obtained from N_2 adsorption-desorption for all ACMs

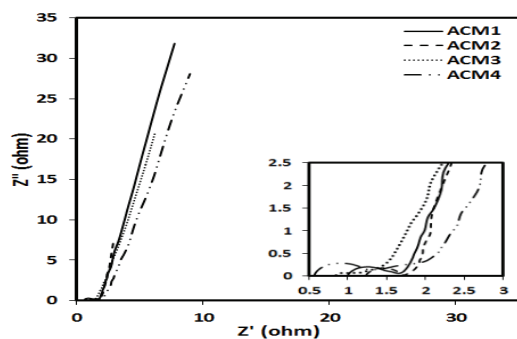| Sample	ACM1	ACM2	ACM3	ACM4
S_{BET} (m^2g^{-1})	459	465	420	481
S_{Meso} (m^2g^{-1})	27	42	44	39
S_{Micro} (m^2g^{-1})	431	424	375	442
V_{Meso} (cm^3g^{-1})	0.019	0.027	0.021	0.023
V_{Micro} (cm^3g^{-1})	0.203	0.199	0.175	0.208
D (Å)	19.2	19.5	19	19.2

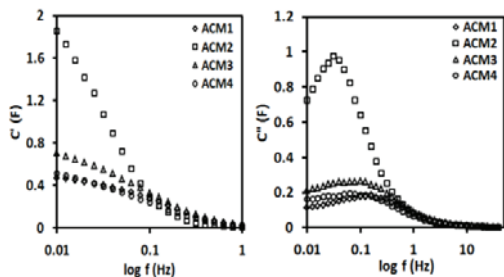**FIGURE 4.** Nyquist plot for ACM1 to ACM4 cells.

FIGURE 5. Capacitance of the (a) real part and (b) imaginary part dependence on frequencies for ACM1 to ACM4 cells.

Cyclic voltammogram for each cell with different carbonization temperatures over a potential range of 0-1 V and scan rate of 1 mV/s are shown in Figure 6. Scan rate of 1 mV/s was choosen because it can provide sufficient time for ions to enter the pores completely compared to larger scan rate [17,18]. Each cell exhibit a similar window with a parallelogram like-shaped, indicating that each cell has a similar characteristic of double-layer capacitor has a highly reversible property, pure electrostatic and non-faradaic reaction mechanism (non-pseudocapacitance) and stability in acidic solution [19]. Although all the window have a similar shape but their area are

different, which is an evident of the effect arising from the different in carbonization temperature. The largest area is shown by the cell ACM2 and hence its specific capacitance value, calculated using equation (2), is higher compared to the other cells (Table 4).

TABLE 3. Values of R_s, R_p, f_p and τ_o for ACM1 to ACM4 cells

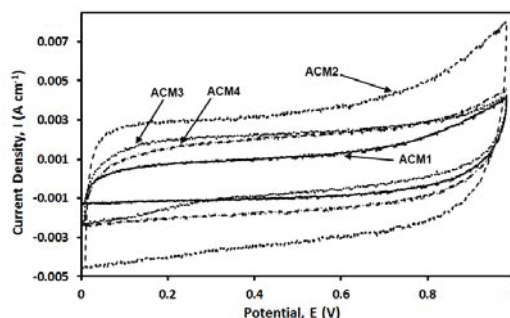| Sample	R_s(ohm)	R_p(ohm)	f_p (Hz)	τ_o (s)
ACM1	0.5372	1.1256	0.1585	6.301
ACM2	0.5688	1.0422	0.0316	31.63
ACM3	0.5465	0.9179	0.1	10
ACM4	0.5621	1.2769	0.0631	16.39

FIGURE 6. Cyclic voltammetry (CV) for ACM1 to ACM4 cells.

Figure 7 shows that each cell shows a typical shape of GCD curves recorded at 10 mA/cm^2 current density from carbon based supercapacitor but their charge-discharge period differ for different carbonization temperatures. ACM2 cell recorded the longest charge-discharge periods and obviously produced the highest specific capacitance, as shown by the results calculated from GCD data using equation (3) in Table 4.

The specific energy and the specific power for each cell, calculated using equations (4) and (5) respectively, are shown as Ragone plot in Figure 8. It is clearly shown that the change in carbonization temperature causes a significant change in the specific energy-specific power relationship. Comparing to other cells, ACM2 cell seems to have a significantly larger maximum specific energy whereas its maximum specific power seem to be relatively close to other. The relaxation time (τ_o) results obtained earlier was used to analyze the maximum specific energy and power of the cells and a consistent result was observed. A similar result was observed on supercapacitor using different type of carbon electrode [20,21].
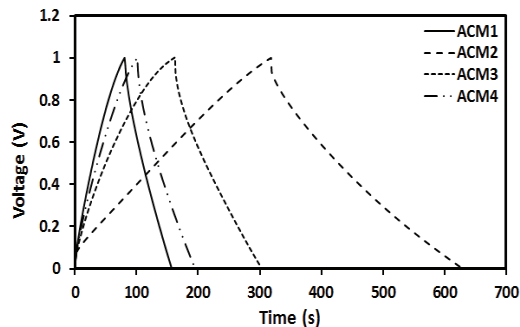
FIGURE 7. GCD curves at 10 mA/cm^2 current densities for ACM1 to ACM4 cells.
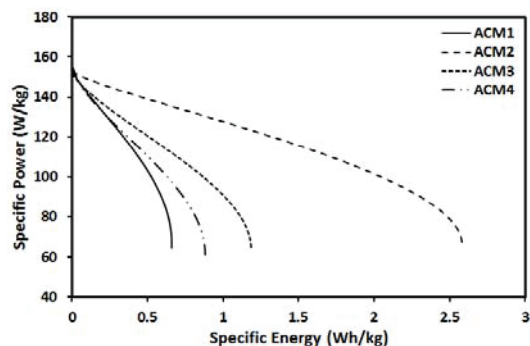

FIGURE 8. Specific power against specific energy or Ragone plot for each cell.

TABLE 4. Values of specific capacitance calculated from EIS^x, CV^y and GCD^z data

Sample	C$_{sp}$^{x} (F/g)	C$_{sp}$^{y} (F/g)	C$_{sp}$^{z} (F/g)	E^z (Wh/kg)	P^z (W/kg)
ACM1	17	36	26	0.6743	158.87
ACM2	71	112	108	2.5825	152.52
ACM3	26	62	49	1.1866	151.78
ACM4	19	50	40	0.8811	155.67

CONCLUSION

Carbon electrodes for supercapacitor application were prepared from pre-carbonized fiber of oil palm empty fruit bunches by carbonization at (400-700°C) and followed by CO$_2$ activation at 800°C. The change in carbonization temperature was found to affect the physical and electrochemical properties of the electrodes. Characterization by EIS, CV and GCD methods consistently show that electrode prepared via 500°C carbonization temperature exhibit superior performance compared to those prepared with other carbonization temperatures.

ACKNOWLEDGMENTS

REFERENCES

1. A. G. Pandolfo and A. F. Hollenkamp, *J. Power Sources* **157**, 11-27 (2006).
2. J. I. Kim, K. Y. Rhee and S. J. Park, *J. Coll. Sci. Interf. Sci* **377**, 307-312 (2012).
3. A. Burke, *J. Power Sources* **91**, 37-50 (2000).
4. A.B.Fuertes, G.Lota, T.A. Centeno and E. Frackowiak, *Electrochim. Acta* **50**, 2799-2805 (2005).
5. E. Taer, M. Deraman, I. A. Talib, Awitdrus, S. A. Hashmi, and A. A. Umar, *Int. J. Electrochem. Sci* **6**, 3301-3315 (2011).
6. M. Deraman, S. Zakaria, R. Omar and A.A. Aziz, *Jpn. J. Appl. Phys* **39**, L1236-L1238 (2000).
7. Awitdrus, M. Deraman, I. A. Talib, R. Omar, M. H. H. Jumali, E. Taer, and M. M. Saman, *Sains Malays.* **39**(1), 83-86 (2010).
8. M. Deraman, S. Zakaria, and J.A. Murshidi, *Jpn. J. Appl. Phys., Part 1* **40**,3311-3314 (2001).
9. C. Portet, P.L. Taberna, P. Simon, E. Flahaut and C. Laberty-Robert, *Electrochim. Acta* **50**, 4174-4181 (2005).
10. J. M. Boyea, R. E. Camacho, S. P. Turano, and W. J. Ready, *Nanotech L & Bus* **4**(1), 585-593 (2007).
11. Z. Ryu, J. Zheng, M. Wang, and B. Zhang, *Carbon* **37**, 1257-1264 (1999).
12. M. P. Bichat, E. R. Pinero, and F. Beguin, *Carbon* **48**, 4351-4361 (2010).
13. A. Aworn, P. Thiravetyan, and W. Nakbanpote, *Colloid. Surface A* **333**, 19-25 (2009).
14. X. M. Liu, R. Zhang, L. Zhan, D. H. Long, W. M. Qiao, H. H. Yang, and L. C. Ling, *New Carbon Mater.* **22**, 153-158 (2007).
15. H. Yu, J. Wu, L. Fan, K. Xu, X. Zhong, Y. Lin, and J. Lin, *Electrochim. Acta* **56**, 6881-6886 (2011).
16. D. Pech, M. Brunet, H. Durou, P. Huang, V. Mochalin, Y. Gogotsi, P. L. Taberna, and P. Simon, *Nature Nanotech* **162**, 651 (2010).
17. A. Awitdrus, M. Deraman, I.A. Talib. R. Farma, R. Omar, M. M. Ishak, N. H. Basri, and B. N. D. Dolah, *Adv. Mat. Res.* **501**, 13-18 (2012).
18. W-C. Chen, T-C. Wen, and H. Teng, *Electrochim. Acta* **48**, 641-649 (2003).
19. E. Taer, M. Deraman, I.A. Talib, A.A. Umar, M. Oyama, and R. M. Yunus, *Curr. Appl Phys* **10 (4)** 1071-1075 (2010).
20. M. O-Marin, J. A. Fernandez, M. J. Lazaro, C. F-Gonzalez, A. M-Garcia, V. G-Serrano, F. Stoeckli, and T. A. Centeno, *Mater. Chem. Phys* **114**, 323-327 (2009).
21. E. Taer, M. Deraman, I.A. Talib, S.A. Hashmi and A.A. Umar, *Electrochem. Acta* **6**, 3301-3305 (2011).